JACS
JOURNAL OF THE AMERICAN CHEMICAL SOCIETY
pubs.acs.org/JACS
Article

Metformin-Induced Stromal Depletion to Enhance the Penetration of Gemcitabine-Loaded Magnetic Nanoparticles for Pancreatic Cancer Targeted Therapy

Haijie Han,[#] Yi Hou,[#] Xiaohui Chen,[#] Peisen Zhang, Muxing Kang, Qiao Jin,[*] Jian Ji, and Mingyuan Gao[*]

Cite This: J. Am. Chem. Soc. 2020, 142, 4944−4954

Read Online

ACCESS | Metrics & More | Article Recommendations | Supporting Information

ABSTRACT: Pancreatic ductal adenocarcinoma, as one of the most aggressive cancers, is characterized by rich desmoplastic stroma that forms a physical barrier for anticancer drugs. To address this issue, we herein report a two-step sequential delivery strategy for targeted therapy of pancreatic cancer with gemcitabine (GEM). In this sequential strategy, metformin (MET) was first administrated to disrupt the dense stroma, based on the fact that MET downregulated the expression of fibrogenic cytokine TGF-β to suppress the activity of pancreatic stellate cells (PSCs), through the 5′-adenosine monophosphate-activated protein kinase pathway of PANC-1 pancreatic cancer cells. In consequence, the PSC-mediated desmoplastic reactions generating α-smooth muscle actin and collagen were inhibited, which promoted the delivery of GEM and pH (low) insertion peptide (pHLIP) comodified magnetic nanoparticles (denoted as GEM-MNP-pHLIP). In addition, pHLIP largely increased the binding affinity of the nanodrug to PANC-1 cells. The targeted delivery and effective accumulation of MET/GEM-MNP-pHLIP in vivo were confirmed by magnetic resonance imaging enhanced by the underlying magnetic nanoparticles. The tumor growth inhibition of the sequential MET and GEM-MNP-pHLIP treatment were investigated on both subcutaneous and orthotopic tumor mice models. A remarkably improved therapeutic efficacy, for example, up to 91.2% growth inhibition ratio over 30 d of treatment, well-exemplified the novel cascade treatment for pancreatic cancer and the innovative use of MET.

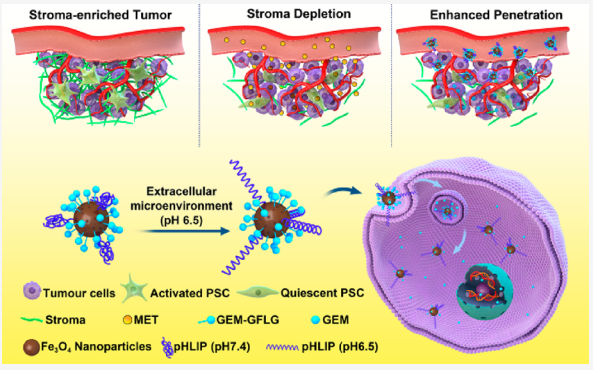

INTRODUCTION

Pancreatic ductal adenocarcinoma (PDAC) is an extremely malignant cancer with an overall five-year survival rate lower than 10%.[1,2] PDAC does not show any symptoms until reaching advanced stages, which makes the early diagnosis extremely difficult. In consequence, most PDAC patients are restricted to chemotherapy, because they are not eligible for surgical resection anymore.[3]

Gemcitabine (GEM), a cytidine nucleoside analogue, has become the standard first-line treatment of PDAC since 1977. However, because of very fast metabolic deactivation by cytidine deaminase, the clinical performance of GEM remains poor, with median survival time only extendable for a few weeks.[4,5] Loading chemotherapeutic drugs with nanocarriers has been proposed, because improved stability and tunable releasibility, apart from the increased half-life and tumor concentration of the loaded drugs, are reasonably expected in vivo.[6−9] Nevertheless, the therapeutic performance of GEM-loaded nanoagents against PDAC remains unsatisfactory.

In fact, PDAC as the most stroma-rich cancer contains as high as 90% stroma besides ∼10% cancer cells.[10,11] Pancreatic stellate cells (PSCs) play a critical role in establishing the stromal compartment of PDAC. Upon activation by profibrogenic mediators such as transforming growth factor β (TGF-β), PSCs will secrete excessive extracellular matrix (ECM) proteins, including collagen, fibronectin, laminin, and glycoproteins, which are the predominant source of stroma. The dense stroma produced by PSCs leads to high interstitial fluid pressure, which severely hinders the effective extravasation of therapeutic (nano)agents from blood vessels to tumor tissues. Moreover, the abundant stromal cells form a physical barrier, together with the high-density ECM, to inhibit the penetration of given (nano)drugs for PDAC treatment.[12−14] Different strategies, including vascular normalization, degradation of stromal barrier, and inhibition of stromal synthesis, have been considered to remodel the tumor microenvironment

Received: January 17, 2020
Published: February 18, 2020

https://dx.doi.org/10.1021/jacs.0c00650
J. Am. Chem. Soc. 2020, 142, 4944−4954

Scheme 1. Illustration of MET-Induced Stromal Depletion[a]

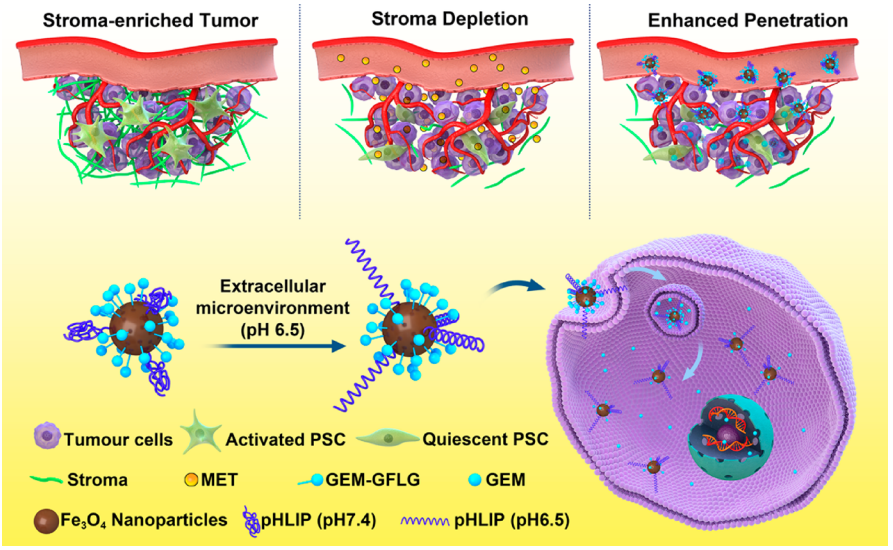

[a]Illustration of MET-induced stromal depletion for enhancing the penetration and cathepsin B-triggered release of gemcitabine carried by Fe_3O_4 nanoparticles in the lysosome of PADC cells.

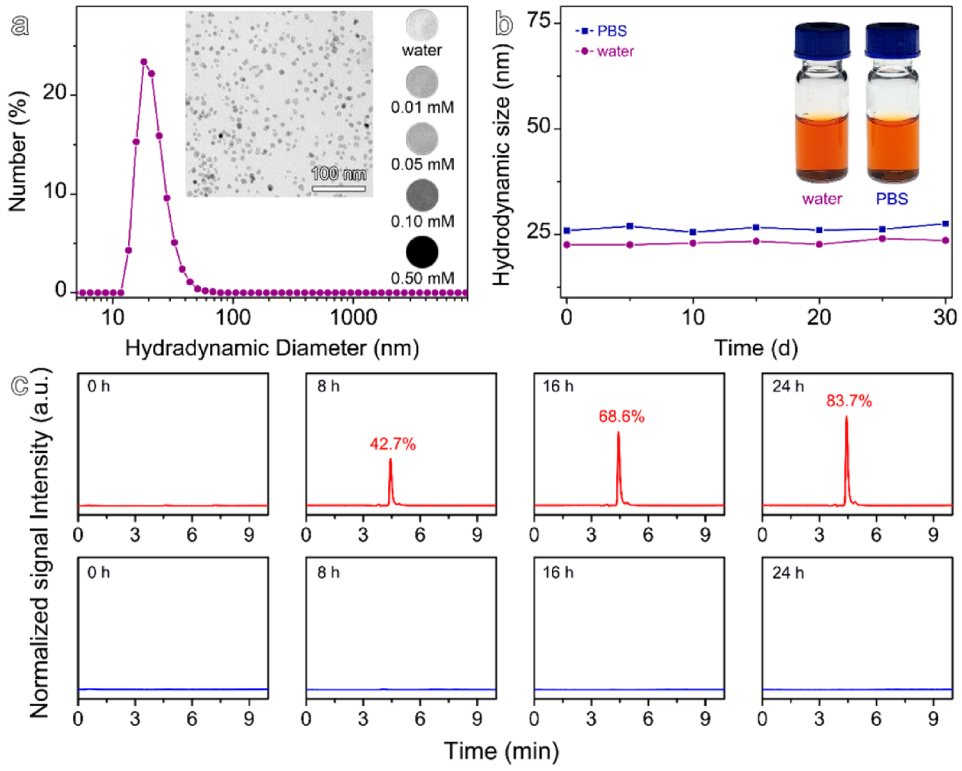

Figure 1. Hydrodynamic size profile of GEM-MNP-pHLIP conjugates in water (a). (inset) TEM image and T_2-weighted images of aqueous solutions containing GEM-MNP-pHLIP with different Fe concentrations as indicated. Temporal hydrodynamic sizes of the GEM-MNP-pHLIP conjugates in water and PBS buffer, respectively (b), and HPLC traces showing the release of GEM upon incubation in the presence (upper) or absence (lower) of cathepsin B at pH 5.5 for different periods of times (the concentration of GEM-MNP-pHLIP with respect to GEM was of 0.1 mg mL^{-1}, and the concentration of cathepsin B was of 0.5 UN mL^{-1}) (c).

for optimizing the pharmacokinetic behaviors of nanodrugs.[15−24] For example, nanoparticles of semiconducting polymer with photothermic activity in response to near-infrared irradiation were used to digest collagen for enhancing the tumor accumulation of particles.[25] Quercetin nanoparticles were reported to modulate the tumor microenvironment for improving the penetration of cisplatin nanoparticles in bladder cancer therapy.[26] Vitamin D receptor-mediated stromal reprogramming showed great potentials in improving pancreatic cancer therapy.[27] The blockade of TGF-β was considered as an effective way to remodel the tumor microenvironment for potentially improving the therapeutic efficacy of many kinds of cancers.[28,29] All above studies suggest that stroma-selective

https://dx.doi.org/10.1021/jacs.0c00650
J. Am. Chem. Soc. 2020, 142, 4944−4954

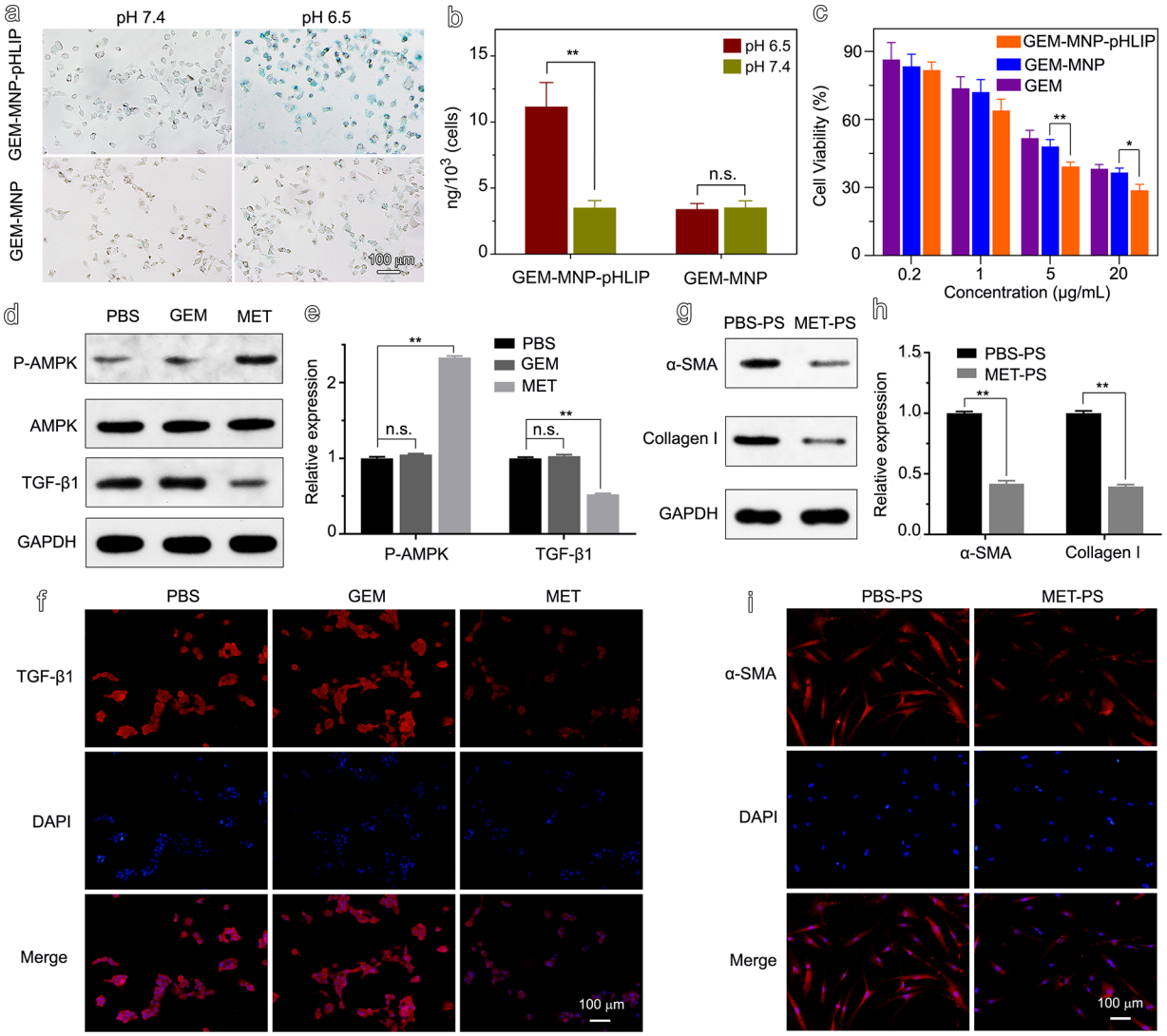

Figure 2. (a) Prussian Blue staining and (b) Fe concentration of PANC-1 cells incubated for 4 h with GEM-MNP-pHLIP and GEM-MNP (10 mg Fe L^{-1}) at pH 7.4 and 6.5, respectively (n = 4). (c) The viability of PANC-1 cells treated with GEM, GEM-MNP, and GEM-MNP-pHLIP, respectively, at pH 6.5 for 72 h (n = 4). (d) Western blot results of MPK, P-MKP, and TGF-β1 levels after PANC-1 cells were incubated with 10 μM GEM or 5 mM MET for 24 h. (e) Quantitative analysis of P-AMKP and TGF-β1 levels from western blot assay. (f) Immunofluorescent images of TGF-β1 protein in PANC-1 cells after treated with 10 μM GEM or 5 mM MET for 24 h. (g) Western blot assay shows the expression of α-SMA and collagen I in PSCs. PSCs were incubated with MET-treated supernatant of PANC-1 cells (MET-PS) or PBS-treated supernatant of PANC-1 cells (PBS−PS) for 24 h. (h) Quantitative analysis of α-SMA and collagen I levels from western blot assay. (i) Immunofluorescent images of α-SMA in PSCs after PSCs were treated with PANC-1 cells-derived supernatants for 24 h. * $p < 0.05$, ** $p < 0.01$.

modulation may provide a promising avenue toward improved PDAC treatment by further taking advantage of nanodrugs.

Metformin (MET), a commonly prescribed antidiabetic drug, is recently receiving increasing attention in suppressing cancer initiation and progression.[30−33] MET can suppress tumor growth by activating adenosine monophosphate-activated kinase (AMPK) pathway and subsequent p53 pathway, inhibiting the electron transport chain (ETC) and adenosine triphosphate (ATP) synthesis, suppressing ERK/P70S6K signaling, and so on.[34−36] The AMPK pathway is closely related with desmoplastic reaction by downregulating TGF-β, which plays an important role in the synthesis of extracellular matrix.[37,38] Therefore, MET might be a potential candidate as a stromal modulator to remodel the tumor microenvironment for improving the penetration of chemotherapeutic nanodrugs in PDAC therapy, which has never been reported.

Toward efficient treatment of PDAC, we herein propose a sequential therapy combining a smart and innovative GEM nanocarrier with MET to facilitate the delivery of GEM and eradicate the tumor burden. Specifically, MET is adopted to inhibit the production and secretion of TGF-β via the AMPK pathway of PANC-1 cells for promoting the stromal depletion by inhibiting the activity of PSCs. The smart nanocarrier comprising of pH-responsive transmembrane unit and controlled release unit, apart from Fe_3O_4 nanoparticles (MNPs) that can be used for monitoring the targeted drug delivery through magnetic resonance imaging (MRI), was designed. It was then prepared by covalently conjugating pH (low) insertion peptide (pHLIP)—a water-soluble membrane peptide and GEM via a cathepsin B-cleavable GFLG peptide sequence to the surface of MNPs. The pHLIP is known to gain transmembrane ability in acidic tumor microenvironment owing to the formation of stable transmembrane α-helix that

https://dx.doi.org/10.1021/jacs.0c00650
J. Am. Chem. Soc. 2020, 142, 4944−4954

facilitates the internalization of the underlying nanoparticles by inserting into cell membranes, on account of the protonation of aspartate and glutamate residues.[39−41] Once internalized into the cancer cells, GEM will be released in lysosome upon cleavage of its linker (i.e., GFLG peptide) by cathepsin B. In the animal experiments, MET was intraperitoneally injected to deplete the dense stromal barrier of PDAC prior to the injection of the above nanoagents to facilitate the effective delivery of GEM. The overall concept and working mechanism are schematically given in Scheme 1.

RESULTS AND DISCUSSION

PEGylated Fe_3O_4 nanoparticles with surface carboxyl groups stemming from the poly(ethylene glycol) (PEG) ligands were prepared through the pyrolysis of ferric acetylacetonate in the presence of α,ω-dicarboxyl-terminated PEG according to our previous work.[42] The PEGylated MNPs dispersed in water showed a number-averaged hydrodynamic size of 18.9 nm (Figure S1). A cathepsin B cleavable GEM derivative, that is, GEM-GFLG-NH_2 and pHLIP (NH_2-AEQNPIYWARYADWLFTTPLLLLDLALLVDADEGT), were then conjugated to the surface of MNPs via amidation reaction, as confirmed by Fourier transform infrared spectroscopy (FTIR) and thermogravimetric analysis (TGA) results given in Figures S2 and S3. Further high-performance liquid chromatography (HPLC) analysis revealed that each nanoparticle carried ∼137 GEM and 11 pHLIP molecules on average, which increases the hydrodynamic size to 22.9 nm as shown in Figure 1a, larger than that determined with transmission electron microscopy (TEM), that is, 10.3 ± 1.1 nm, owing to the hydration of the surface PEG ligands. To evaluate the MRI contrast enhancement effect of the GEM-MNP-pHLIP conjugates, a series of aqueous solutions of the conjugates with Fe concentration ranging from 0.01 to 0.5 mM was prepared and then subjected to T_2-weighted MR imaging (inset of Figure 1a). By fitting the curves of $1/T_1$ and $1/T_2$ against Fe concentration, the molar relaxivities of r1 and r2 were extracted as 6.7 and 153.5 mM^{-1} S^{-1}, respectively. It is worth mentioning that the GEM-MNP-pHLIP conjugates exhibit excellent colloidal stability in both water and phosphate buffered saline (PBS), as the hydrodynamic sizes in both media remain nearly unchanged over 30 d (Figure 1b).

The target-triggered release of GEM is an essential part of the current design, because GEM is prone to be metabolized by cytidine deaminase during blood circulation. On this account, GEM was conjugated to MNPs, hopefully to improve its metabolic stability, via the GFLG linker, which is cleavable between phenylalanine and leucine by cathepsin B overexpressed in pancreatic cancer cells. To verify the target-triggered release, HPLC was used to quantitatively detect the released GEM after the GEM-MNP-pHLIP conjugates were incubated with cathepsin B. As shown in Figure 1c, 42.7%, 68.6%, and 83.7% of the loaded GEM was released over 8, 16, and 24 h of incubation, respectively, while no GEM was detected if the conjugates were incubated in the absence of cathepsin B. Since cathepsin B is overexpressed in cancer cells, GEM-MNP-pHLIP conjugates can achieve minimal drug leakage during circulation and simultaneously effective drug release in the targeted site, which is crucial in reducing the side effects of GEM.

Owing to the pH-dependent configuration, pHLIP as well as the GEM-MNP-pHLIP conjugates are expected to gain active targeting ability to tumor cells at acidic pH. To demonstrate this ability, GEM-MNP-pHLIP conjugates were incubated with PANC-1 cells for 4 h at pH 7.4 and 6.5, respectively. In parallel, MNPs solely modified with GEM (i.e., GEM-MNP) were prepared, according to the same procedures for GEM-MNP-pHLIP conjugates, except that pHLIP was not added (Figure S4) and was used as control. The cancer cells were then subjected to Prussian Blue staining to show the influence of pH on the internalization of MNPs, as given in Figure 2a. The concentration of Fe in the cells was quantitatively determined by inductively coupled plasma mass spectrometry (ICP-MS). As presented in Figure 2b, the cellular uptake of the GEM-MNP conjugates was nearly pH-independent at pH 7.4 and 6.5, which indicated that the solution pH hardly affected the internalization ability of PANC-1 cells in the absence of pHLIP. However, the quantity of GEM-MNP-pHLIP conjugates uptaken by PANC-1 cells at pH 6.5 was 3.2-fold higher than that obtained at pH 7.4. Meanwhile, the cellular uptake of the GEM-MNP conjugates at pH 6.5 is as low as that of GEM-MNP-pHLIP conjugates at pH 7.4, suggesting that lowering pH can promote the cell binding affinity of the GEM-MNP-pHLIP conjugates to PANC-1 cells. Therefore, GEM-MNP-pHLIP conjugates exhibit enhanced cellular uptake in acidic tumor microenvironment due to pH-dependent configuration of pHLIP, which plays a key role in efficient tumor retention and enhanced cytotoxicity.

The methyl thiazolyl tetrazolium (MTT) method was adopted to study the cell viability after different treatments. The blank nanocarriers without GEM conjugation (MNP-pHLIP) did not show any toxicity toward human umbilical vein endothelial (HUVEC) cells, indicating excellent biocompatibility of the mother MNPs (Figure S5). Meanwhile, after incubation of MNP-pHLIP with PANC-1 cells at pH 7.4 and 6.5, the viability of PANC-1 cells was not affected by solution pH and concentration of MNP-pHLIP, ruling out the effects of solution pH and the mother MNPs on the viability of PANC-1 cells (Figure S6a). Compared with GEM-MNP conjugates, the GEM-MNP-pHLIP conjugates exhibited higher cytotoxicity at pH 6.5, which was probably caused by the enhanced cellular uptake of the GEM-MNP-pHLIP conjugates in acidic pH (Figure 2c). At the same time, the cytotoxicity of GEM-MNP conjugates was almost unchanged from pH 7.4 to 6.5 (Figure S6b). However, the GEM-MNP-pHLIP conjugates exhibited higher cytotoxicity at pH 6.5 than that at pH 7.4, which might be attributed to pH-dependent enhanced cellular uptake (Figure S6c). To investigate the effect of cathepsin B-triggered drug release, PANC-1 cells were pretreated with cathepsin B inhibitor CA-074Me to downregulate intracellular cathepsin B. As shown in Figure S7, the cytotoxicity of GEM-MNP-pHLIP conjugates is greatly suppressed, indicating that the efficient drug release is very important for inhibiting cancer cell proliferation. Another proof came from the much lower cytotoxicity of GEM-MNP-pHLIP conjugates to HUVEC cells owing to the low cathepsin B level in the latter cells, which indicated low side effects of GEM-MNP-pHLIP conjugates (Figure S8). Therefore, pHLIP-triggered cellular uptake and cathepsin B-sensitive drug release of GEM are rationally integrated for achieving enhanced anticancer capacity and reduced side effects.

It is known that the dense stroma of PDAC is a serious obstacle in chemotherapy.[10] The antistromal therapeutic strategy has therefore become a hot topic in PDAC therapy in recent years.[19,27] The activation of AMPK pathway plays an important role in inhibiting desmoplastic reaction.[38] Therefore,

https://dx.doi.org/10.1021/jacs.0c00650
J. Am. Chem. Soc. 2020, 142, 4944−4954

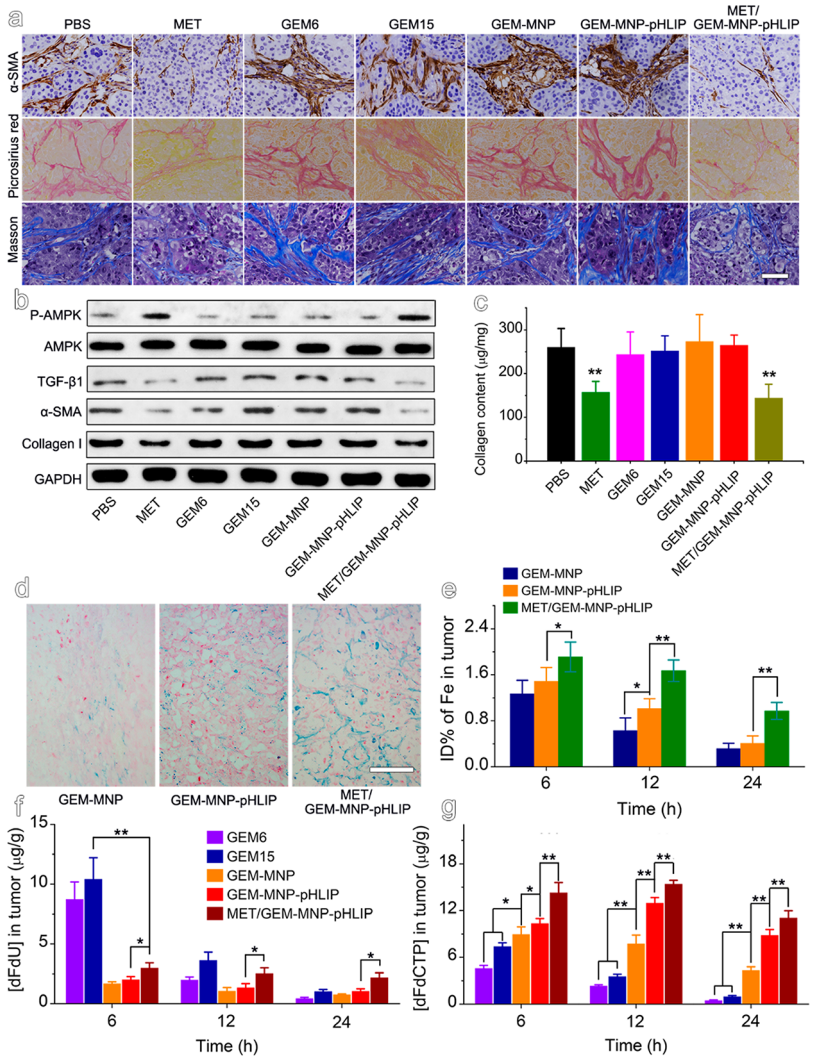

Figure 3. (a) Tumor tissues subjected to immunohistochemical staining (α-SMA), Picrosirius red staining, and Masson's trichrome staining after receiving different treatments as indicated (scale bar: 50 μm). (b) Western blot results of the expression of AMPK, P-AMPK, TGF-β1, α-SMA, and collagen I of tumor tissues receiving different treatments as indicated. (c) Collagen content in tumor tissues was determined through Sircol collagen assay after receiving different treatments as indicated (n = 5). (d) Prussian Blue staining of tumor tissues after receiving different treatments 12 h postinjection. Scale bar: 100 μm. (e) Fe content in tumor tissues after different treatments was determined through ICP-MS (n = 5). (f) Temporal evolution of dFdU in tumor tissues after receiving different treatments as indicated (n = 5). (g) Temporal evolution of dFdCTP in tumor tissues after receiving the treatments indicated in frame f (n = 5). * $p < 0.05$, ** $p < 0.01$.

it is interesting to show the effect of MET on the AMPK signaling pathway. Because the phosphorylation of AMPK is a necessary step to activate the loop of AMPK, the AMPK and phosphorylated-AMPK (P-AMPK) levels were then determined after PANC-1 cells were treated with MET. As shown in Figure 2d,e, GEM treatment cannot affect the AMPK and P-AMPK level. However, a 2.3-fold increase in P-AMPK level was observed after PANC-1 cells were incubated with 5 mM MET for 24 h, indicating that MET can activate the AMPK pathway. The activation of AMPK pathway is known to be related with TGF-β induced fibrogenesis.[43] As expected, the expression level of TGF-β, a very important cytokine that plays a critical role in fibrotic processes,[44] was also found to decrease by 47.6% according to the western blot assays (Figure 2d,e), which was further confirmed by immunofluorescent imaging (Figure 2f). The following enzyme-linked immunosorbent assay (ELISA) results revealed that concentration of TGF-β1 in the cell culture media was decreased from 418.6 pg per 10^5 cells to 217.5 pg per 10^5 cells (Figure S9). It is known that TGF-β as the most important mediator for PSCs activation can stimulate the activated PSCs to secrete excessive extracellular matrix proteins.[45,46] Since production and secretion of TGF-β can be inhibited by MET, it is interesting to show the effects of MET on the interaction between PANC-1 cells and PSCs in tumor stroma. To do so, PANC-1 cells were incubated with 5 mM MET for 24 h with PBS as control. Then, the resulting supernatant of the cell culture media was collected and incubated with PSCs for another 24 h. The α-smooth muscle actin (α-SMA) and collagen I secreted by PSCs were determined by western blot assay. As presented in Figure 2g–i, the expression level of α-SMA and collagen I was reduced by 58.1% and 60.4%, respectively, after the PSCs were incubated with supernatant of PANC-1 cells receiving MET treatment. However, the α-SMA level was not changed if PSCs were directly incubated with 5 mM MET (Figure S10). Therefore, it can be concluded that MET cannot directly stimulate PSCs to inhibit the stromal formation. However, MET can stimulate PANC-1 cells to inhibit the secretion of

https://dx.doi.org/10.1021/jacs.0c00650
J. Am. Chem. Soc. 2020, 142, 4944–4954

TGF-β. As TGF-β plays a critical role in PSCs-mediated stromal reaction by regulating α-SMA expression and collagen I synthesis,[13] MET exhibits remarkable inhibition effects on PSCs-mediated stromal synthesis.

On the basis of the above in vitro cell studies, it is interesting to show if MET can deplete the dense stromal barrier to promote the penetration of GEM-loaded MNPs for improving the treatment of PDAC. The oncotherapy experiments were then conducted on stromal-rich PDAC mouse model established by subcutaneously inoculating a mixture of PANC-1 cells and PSCs (2:1).[21] The tumor-bearing nude mice were randomly divided into seven groups. Six of them were treated with PBS (control), MET (100 mg/kg), low-dosage GEM (GEM6, 6 mg/kg body weight), high-dosage GEM (GEM15, 15 mg/kg), GEM-MNP (GEM, 6 mg/kg), and GEM-MNP-pHLIP (GEM, 6 mg/kg), respectively. The last group was sequentially treated with MET followed by GEM-MNP-pHLIP (MET/GEM-MNP-pHLIP, 6 mg/kg GEM). The treatment effects on stroma are shown in Figure 3. For example, the untreated stroma (PBS group) is dense and well-organized as depicted by α-SMA brown staining, rather similar to the structure of collagen fibers outlined by Picrosirius red and Masson staining (Figure 3a). However, the collagen fibers in tumor tissue were remarkably decreased upon treatment with MET (i.e., MET and MET/GEM-MNP-pHLIP group), strongly indicating that the dense stroma was obviously disrupted, while the tumor stroma from the remaining four groups remains almost unchanged.

To disclose the underlying molecular mechanism for stromal modulation induced by MET in vivo, western blot studies were performed at first to show its effect on the expression levels of AMPK and P-AMPK. The results given in Figure 3b and Figure S11 apparently support that MET can effectively activate the AMPK pathway as it does for PDAC cells in vitro. Twofold increase of P-AMPK level was observed when the mice were treated with MET, while the remaining four groups did not show obvious change in P-AMPK expression. The expression level of TGF-β1 determined in tumor tissue was found to be decreased by 40% upon MET treatment, indicating that TGF-β expression can effectively be inhibited by MET in vivo.

To quantitatively analyze the collagen content upon MET treatment, the tumor tissues extracted after different treatments were subjected to Sircol assay. As shown in Figure 3c, MET treatment can reduce the collagen content by up to 40%, well in accordance with western blot and immunohistochemistry results. Therefore, it can be concluded that MET treatment can effectively activate AMPK pathway and then downregulate the expression of TGF-β in tumor tissue in vivo, leading to the inhibition of α-SMA expression and collagen I synthesis. In this context, MET treatment is reasonably expected to deplete the dense stroma of PDAC to facilitate the delivery GEM carried by MNP nanocarriers.

To verify the effect of MET treatment on the penetration efficacy of nanoparticles, the tumor tissues from mice receiving different treatments were stained with Prussian Blue to show the impact of MET on the eventual accumulation of MNPs in tumors. Apparently, as shown in Figure 3d, the accumulation of MNPs in tumor tissues is increased if comparing GEM-MNP-pHLIP group with GEM-MNP group. Interestingly, the accumulation of MNPs in tumor tissues can further be increased if MET is administrated prior to the GEM-MNP-pHLIP conjugates (MET/GEM-MNP-pHLIP). This tendency is quantitatively confirmed by ICP-MS analysis on the Fe content of tumors in mice receiving the corresponding treatments. As shown in Figure 3e, the Fe accumulation in tumors from MET/GEM-MNP-pHLIP group is increased by a factor of 2.4 in comparison with that from GEM-MNP-pHLIP group 24 h postinjection. The temporal variation of Fe content also reflects the retention of the nanodrugs. For example, the Fe content drops by 49.2% from 6 to 24 h postinjection for MET/GEM-MNP-pHLIP group, much smaller than 68.3% for GEM-MNP-pHLIP group and 75.6% for GEM-MNP group. The enhanced retention of MNPs from GEM-MNP-pHLIP group, compared with that from GEM-MNP group, can reasonably be attributed to pHLIP that gains transmembrane ability in acidic environment and consequently enhances the uptake of the underlying MNPs, while the remarkably increased penetration and retention of MNPs in the MET/GEM-MNP-pHLIP group strongly supports that MET can effectively increase the tumor accumulation of MNPs loaded with GEM by depleting the dense stromal barrier of PDAC.

Combination therapy is regarded as an indispensable strategy for cancer therapy in clinical practice.[47] However, the sequence of combination treatments is very critical for satisfying the spatiotemporal needs of each drug due to their differences in pharmacokinetics, mechanism of action, and action sites.[48,49] In this context, it is interesting to know if the cascade treatment based on sequential administrations of MET and pHLIP prodrug can effectively suppress the deaminization of GEM in vivo. In principle, GEM undergoes two different metabolic pathways in vivo, that is, being converted into inactive 2′,2′-difluorodeoxyuridine (dFdU) by cytidine deaminase or being phosphorylated into triphosphate form (dFdCTP) that kill cancer cells by inhibiting ribonucleotide reductase.[5] To disclose the pathway dominating the metabolism of GEM loaded by MNPs, quantitative analysis on dFdU and dFdCTP in tumor tissues of mice receiving different treatments was performed by HPLC. The results shown in Figure 3f,g reveal that free GEM is prone to be transformed into dFdU rather than dFdCTP in tumor in vivo. For example, the dFdU concentration in GEM6 group is 4.3-fold of that of GEM-MNP-pHLIP group 6 h postinjection, and the dFdCTP concentration is only half of that from the latter group, suggesting that the immobilized GEM is more metabolically stable than free GEM. This can probably be interpreted by the fact that the cytidine deaminase/GEM binding site is taken by the conjugation of GEM to MNPs, which increases the metabolic stability of immobilized GEM in vivo. Moreover, the MET pretreatment further raises the dFdCTP concentration in tumor if GEM-MNP-pHLIP treatment is followed. As a result, the MET/GEM-MNP-pHLIP group presents the highest dFdCTP concentration, ~20-fold higher than that of the free GEM groups (i.e., GEM 6 and GEM 15) 24 h postinjection. This dramatically increased dFdCTP concentration can reasonably be attributed to both enhanced penetration through the tumor stroma barrier and improved internalization into PANC-1 cells of the GEM-MNP-pHLIP conjugates, in consequence of MET pretreatment.

All this evidence suggests that combination of GEM-MNP-pHLIP prodrug with MET may maximize the therapeutic efficacy of GEM by avoiding its deamination. To show the anticancer performance of this cascade treatment, the in vivo oncotherapy experiments were then performed with different formulations based on the major components of the GEM-MNP-pHLIP conjugates and MET as well. As shown in Figure

https://dx.doi.org/10.1021/jacs.0c00650
J. Am. Chem. Soc. 2020, 142, 4944−4954

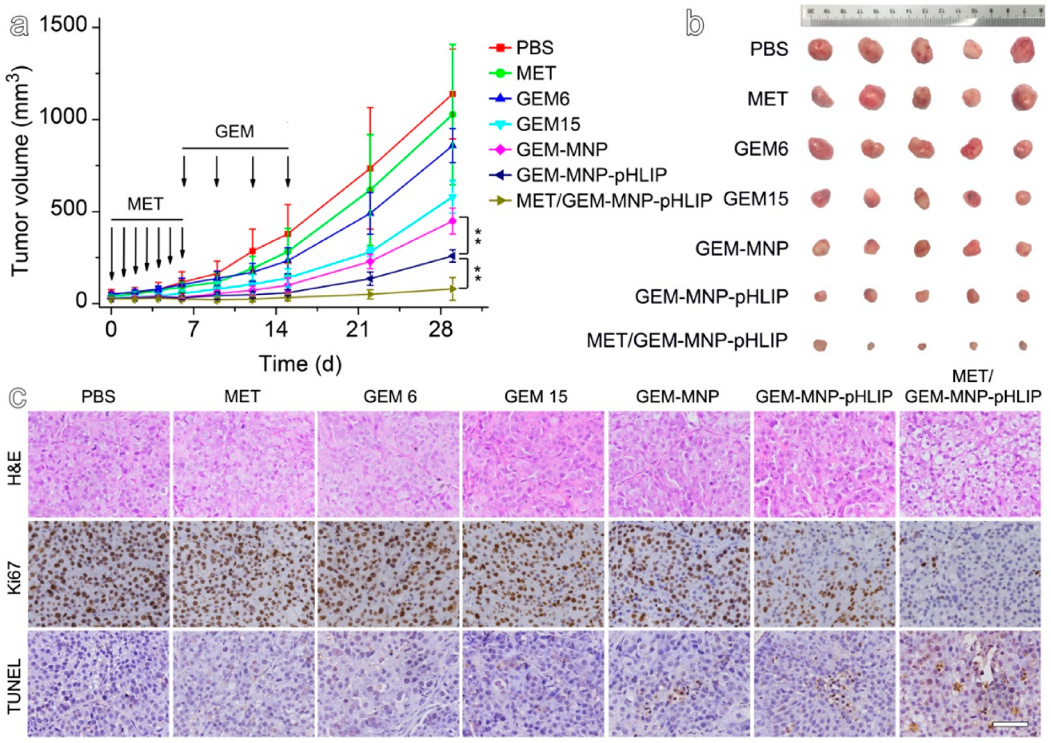

Figure 4. (a) Tumor growth inhibition curves for PANC-1 subcutaneous xenografts borne by nude mice receiving different treatments as indicated (n = 5) (the tumor volume was calculated by length × width/2). (b) Photographs of the tumors extracted on T+30 d after receiving different treatments as indicated. (c) H&E, Ki67, and TUNEL staining of the corresponding tumor tissues obtained after different treatments. The embedded scale bar corresponds to 100 μm. * $p < 0.05$, ** $p < 0.01$.

4a, MET and GEM6 groups present little tumor inhibition effect in comparison with PBS group. This effect is enhanced by increasing the concentration of GEM up to 15 mg/kg (GEM15 group), while it is still weaker than those obtained with the nanodrug groups, that is, GEM-MNP, GEM-MNP-pHLIP, and MET/GEM-MNP-pHLIP. The enhanced therapeutic efficacy in nanodrug groups might be ascribed to the effective tumor accumulation and inhibition of GEM deaminization. In addition, among all the nanoprodrug groups, the MET/GEM-MNP-pHLIP group apparently exhibits the best therapeutic efficacy as shown in Figure 4a,b, which can be quantitatively expressed by tumor growth inhibition ratio (TIR) given in Figure S12. Over 30 d treatments, the TIR ratio was calculated to be 91.2%, 77.3%, 60.7%, 49.1%, 24.7%, and 9.8% for MET/GEM-MNP-pHLIP, GEM-MNP-pHLIP, GEM-MNP, GEM15, and GEM6, respectively.

The antitumor effect of different treatments was also investigated by analyzing the proliferation and apoptosis levels in tumor tissues using immunohistochemistry, including hematoxylin-eosin (H&E) staining, Ki67 assay, and terminal deoxynucleotidyl transferase (TdT)-mediated dUTP nick-end labeling (TUNEL) assay. In brief, the tumor tissue from mice receiving MET/GEM-MNP-pHLIP cascade treatment exhibits the highest apoptosis and lowest proliferation levels, as shown in Figure 4c. Moreover, according to the Ki67 proliferation index and TUNEL apoptosis index as shown in Figures S13 and S14, the MET/GEM-MNP-pHLIP group exhibited the highest therapeutic efficacy, well-consistent with the results given in Figure 4a,b. In addition, the body weight of mice was monitored for evaluating the systemic toxicity of different treatments. As shown in Figure S15, only the high-dosage GEM group (GEM15) led to body weight loss during the treatment, while the remaining groups presented no obvious body weight change in comparison with the PBS control group, indicating low systemic toxicity of the nanoprodrugs.

Encouraged by the outstanding tumor inhibition ability demonstrated on the tumor subcutaneous xenograft tumor model, tumor inhibition studies based on orthotopic pancreatic cancer were performed, as the latter is more clinically relevant. In brief, the mixed cell suspension of PANC-1 cells transfected with a luciferase gene and PSCs was implanted through the tail of pancreas. The detailed treatment procedures are shown in Figure 5a. The mice were randomly divided into seven groups (n = 5). The formation and the following growth of the orthotopic tumors after different treatments were monitored by bioluminescence image (BLI, Figure 5b,c) and MRI (Figure 5d). According to the bioluminescence results shown in Figure 5b,c, MET apparently presents no tumor inhibition function. Although GEM itself can inhibit the tumor growth to some extent, the nanodrug groups exhibit much improved ability in inhibiting tumor growth; particularly the MET/GEM-MNP-pHLIP group gives rise to the most significant tumor growth inhibition as shown in Figures 5e,f and S17. The average tumor weight was 2.01, 1.78, 1.56, 1.28, 1.14, 0.80, and 0.32 g for the mice treated with PBS, MET, GEM6, GEM15, GEM-MNP, GEM-MNP-pHLIP, and MET/GEM-MNP-pHLIP, respectively, which well verify the synergistic effects of MET and GEM-MNP-pHLIP on tumor growth inhibition. In addition, the stromal depletion after MET treatment was also confirmed by immunohistochemistry (Figure S18). The ex vivo histological analyses of tumor tissues indicated that the MET/GEM-MNP-pHLIP group gave rise to the most pronounced apoptosis and lowest proliferation of tumor cells

https://dx.doi.org/10.1021/jacs.0c00650
J. Am. Chem. Soc. 2020, 142, 4944−4954

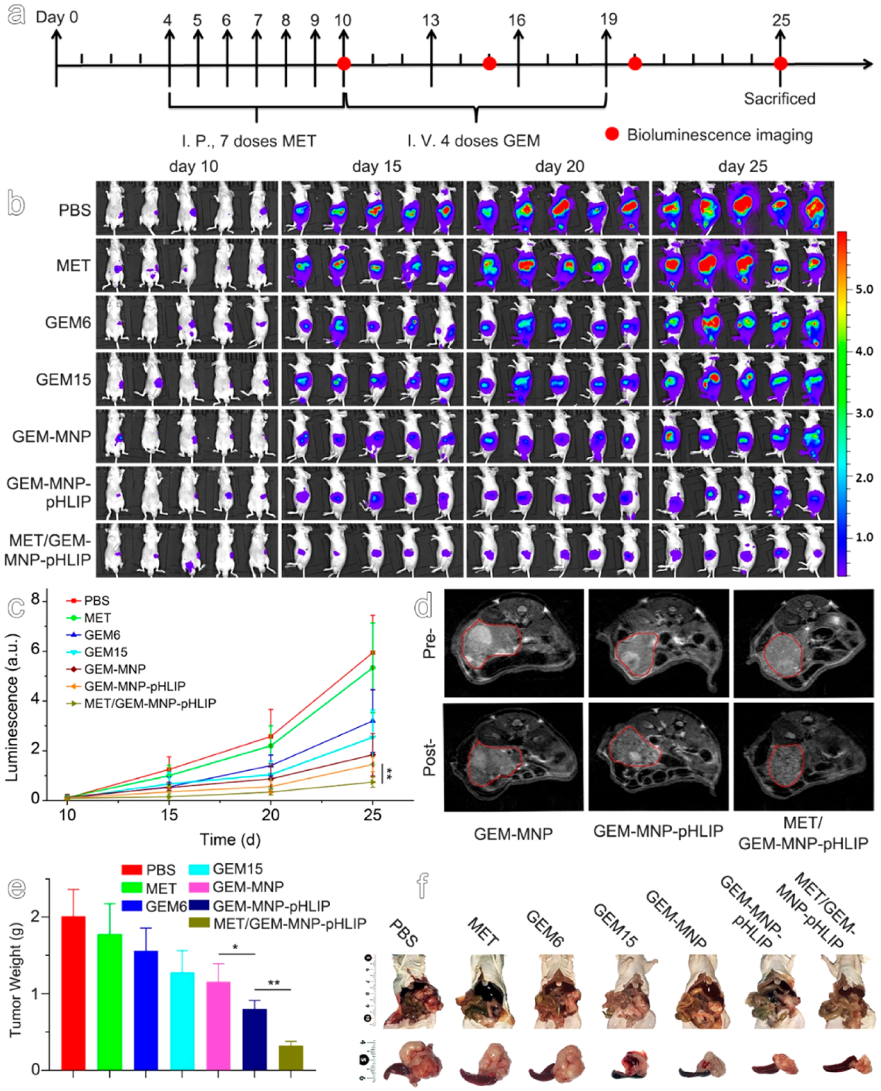

Figure 5. (a) Timeline for orthotopic PDAC tumor-bearing nude mice subjected to different treatments and measurements. (b) Bioluminescence images of different groups of mice recorded at different time points during the treatment. (c) Quantified fluorescent signals of the tumor sites against time after receiving different treatments as indicated (n = 5). (d) T_2-weighted MR images of orthotopic PDAC tumors before and 4 h after receiving different nanodrugs (10 mg of Fe per kilo body-weight) as indicated. (e) The average tumor weights of each group recorded on day 25. (f) Typical bright-field images of tumors with spleens excised on day 25 post-treatment. * $p < 0.05$, ** $p < 0.01$.

(Figures S18−S20), well-consistent with results based on the subcutaneous tumor model.

It is deserved to mention that MNPs possess excellent T_2 contrast enhancement ability apart from acting as a drug carrier,[50−52] which provides the possibility to monitor the delivery of the GEM-MNP-pHLIP prodrug with MRI. As shown in Figure 5d, the precontrasted images of pancreatic tumors present similar T_2-weighted MRI contrast in comparison with the surrounding tissues. However, the contrast of tumorous region is largely increased postinjection of the nanodrugs. Moreover, in comparison with GEM-MNP and GEM-MNP-pHLIP groups, the MET/GEM-MNP-pHLIP group gives rise to the greatest decrease in MRI signal, that is, 37.7% for MET/GEM-MNP-pHLIP versus 20.9% for GEM-MNP-pHLIP and 8.3% for GEM-MNP (Figure S16). The efficient delivery and accumulation of the MNPs in consequence of MET/GEM-MNP-pHLIP treatment manifests well the rationale of the current nanodrug designs for effectively delivering GEM to tumor site.

Actually, the stroma-depleting strategy has been used in clinical studies of pancreatic cancer therapy.[53] For example, PEGylated hyaluronidase PH20 (PEGPH20) was used to digest highly expressed hyaluronan in pancreatic solid tumor to decrease interstitial fluid pressure for drug delivery.[54] Currently, the combination of PEGPH20 with GEM is in Phase III,[55] while the combination of small-molecule smoothened inhibitor LDE225 with GEM is in Phase II clinical trial. As paclitaxel can suppress the formation of stroma,[56] albumin-bound paclitaxel can improve the overall survival of metastatic pancreatic cancer in combination with GEM.[57] MET is a well-known antidiabetic drug with negligible adverse effect. In recent years, MET is receiving more and more attention especially in cancer therapy. For example, the hemin/MET combined therapy exhibited exciting efficacy in triple-negative breast cancer management,[58] while combining MET with hexokinase-2 silencing is very promising in hepatocellular carcinoma therapy.[59] In addition, MET can reverse lung fibrosis and liver fibrosis by activating the AMPK

https://dx.doi.org/10.1021/jacs.0c00650
J. Am. Chem. Soc. 2020, 142, 4944−4954

pathway,[60−62] which supports the use of MET for depleting the stroma of pancreatic cancer toward improved therapy. In fact, both GEM and MET are widely used clinical drugs, and magnetic iron oxide nanoparticle as main component was proved as clinical contrast agent many years ago. Therefore, the current prodrug and the innovative combination of GEM in PADC therapy hold bright futures with respect to translational medicine. To this end, it is necessary to evaluate the biosafety of the GEM-MNP-pHLIP drug. The blood index values of mice receiving different treatments were determined, and the results are listed in Figure S21. In brief, free GEM, especially high-dosage GEM, led to abnormal blood index values for white blood cell (WBC), red blood cell (RBC), blood platelet (PLT), and alanine aminotransferase (ALT). In contrast, GEM loaded by MNPs did not show such side effects. For example, GEM-MNP-pHLIP treatment did not give rise to any noticeable changes through complete blood panel test and serum biochemistry including liver functions and renal functions, which indicated the excellent biocompatibility of the GEM-MNP-pHLIP nanodrug.

CONCLUSIONS

In summary, we have proposed an effective two-step delivery strategy for pancreatic cancer therapy through an innovative combination of metformin with Fe_3O_4 nanocarriers simultaneously immobilized with GEM and pHLIP peptide. In this design, GEM, the widely used antipancreatic cancer drug, is covalently conjugated to the surface of MNPs via the amine group to improve its stability in vivo. Beyond that, it is on-site releasable in response to cathepsin B overexpressed within tumor cells, while the configuration variation of the pHLIP enabled by tumor microenvironment pH largely facilitates the delivery of the nanocarriers loaded with GEM into tumorous regions. The targeted delivery and effective accumulation of MNPs in tumor tissue was confirmed by Prussian Blue staining, ICP-MS analysis, and MRI. Most importantly, to overcome the dense stroma barrier for drug delivery, MET—another clinical drug—is for the first time combined with GEM for improving the delivery efficiency of the latter in vivo. It has been experimentally demonstrated that MET can suppress the production and secretion of TGF-β mediated by PANC-1 cells through AMPK pathway, resulting in the deactivation of PSCs. Then, in consequence of the MET treatment, the inhibited expression of α-SMA and collagen by PSCs gives rise to the depletion of the dense stroma of pancreatic tumor tissue in vivo. With the combination of all the above functions demonstrated both in vitro and in vivo, remarkable tumor inhibitions have been successfully achieved on both mouse subcutaneous and orthotopic tumor model through the sequential treatment of MET and the GEM-MNP-pHLIP nanodrug. We thus believe the current study not only provides an interesting strategy for improving the delivery efficiency of conventional drugs to tumor regions but also expands the applications of MET to efficient treatment of stroma-rich malignancies, especially PDAC, which manifests well the novelty of the current studies.

ASSOCIATED CONTENT

Supporting Information

The Supporting Information is available free of charge at https://pubs.acs.org/doi/10.1021/jacs.0c00650.

Synthesis and characterization of nanoparticles, experimental procedures for the cell studies and animal studies, and more supplementary figures and tables (PDF)

AUTHOR INFORMATION

Corresponding Authors

Qiao Jin − *MOE Key Laboratory of Macromolecule Synthesis and Functionalization of Ministry of Education, Department of Polymer Science and Engineering, Zhejiang University, Hangzhou 310027, P. R. China;* orcid.org/0000-0002-6584-4111; Email: jinqiao@zju.edu.cn

Mingyuan Gao − *Key Laboratory of Colloid, Interface and Chemical Thermodynamics, Institute of Chemistry, Chinese Academy of Sciences, Beijing 100190, P. R. China; State Key Laboratory of Radiation Medicine and Protection, Collaborative Innovation Center of Radiation Medicine of Jiangsu Higher Education Institutions, School for Radiological and Interdisciplinary Sciences, Soochow University, Suzhou 215123, P. R. China;* orcid.org/0000-0002-7360-3684; Email: gaomy@iccas.ac.cn

Authors

Haijie Han − *MOE Key Laboratory of Macromolecule Synthesis and Functionalization of Ministry of Education, Department of Polymer Science and Engineering and Eye Center, the Second Affiliated Hospital, School of Medicine, Zhejiang University, Hangzhou 310027, P. R. China*

Yi Hou − *Key Laboratory of Colloid, Interface and Chemical Thermodynamics, Institute of Chemistry, Chinese Academy of Sciences, Beijing 100190, P. R. China*

Xiaohui Chen − *MOE Key Laboratory of Macromolecule Synthesis and Functionalization of Ministry of Education, Department of Polymer Science and Engineering, Zhejiang University, Hangzhou 310027, P. R. China*

Peisen Zhang − *Key Laboratory of Colloid, Interface and Chemical Thermodynamics, Institute of Chemistry, Chinese Academy of Sciences, Beijing 100190, P. R. China*

Muxing Kang − *Department of Surgery, the Second Affiliated Hospital, School of Medicine, Zhejiang University, Hangzhou 310009, P. R. China*

Jian Ji − *MOE Key Laboratory of Macromolecule Synthesis and Functionalization of Ministry of Education, Department of Polymer Science and Engineering, Zhejiang University, Hangzhou 310027, P. R. China;* orcid.org/0000-0001-9870-4038

Complete contact information is available at: https://pubs.acs.org/10.1021/jacs.0c00650

Author Contributions

#These authors contributed equally.

Notes

The authors declare no competing financial interest.

ACKNOWLEDGMENTS

This work was financially supported by the National Natural Science Foundation of China (21774110, 81530057, 81720108024) and the Fundamental Research Funds for the Central Universities (2019QNA4063, 2019XZZX005-1-03).

REFERENCES

(1) Kleeff, J.; Korc, K.; Apte, M.; La Vecchia, C.; Johnson, C. D.; Biankin, A. V.; Neale, R. E.; Tempero, M.; Tuveson, D. A.; Hruban, R. H.; Neoptolemos, J. P. Pancreatic Cancer. *Nat. Rev. Dis. Primers.* **2016**, *2*, 16022.

(2) Siegel, R. L.; Miller, K. D.; Jemal, A. Cancer Statistics, 2017. *Ca-Cancer J. Clin.* **2017**, *67*, 7−30.

(3) Tempero, M. A.; Berlin, J.; Ducreux, M.; Haller, D.; Harper, P.; Khayat, D.; Schmoll, H. J.; Sobrero, A.; Van Cutsem, E. Pancreatic Cancer Treatment and Research: an International Expert Panel Discussion. *Ann. Oncol.* **2011**, *22*, 1500−1506.

(4) Moysan, E.; Bastiat, G.; Benoit, J. P. Gemcitabine versus Modified Gemcitabine: A Review of Several Promising Chemical Modifications. *Mol. Pharmaceutics* **2013**, *10*, 430−444.

(5) Han, H. J.; Valdepěrez, D.; Jin, Q.; Yang, B.; Li, Z. H.; Wu, Y. L.; Pelaz, B.; Parak, W. J.; Ji, J. Dual Enzymatic Reaction-Assisted Gemcitabine Delivery Systems for Programmed Pancreatic Cancer Therapy. *ACS Nano* **2017**, *11*, 1281−1291.

(6) Peer, D.; Karp, J. M.; Hong, S.; Farokhzad, O. C.; Margalit, R.; Langer, R. Nanocarriers as an Emerging Platform for Cancer Therapy. *Nat. Nanotechnol.* **2007**, *2*, 751−760.

(7) Liu, X.; Situ, A.; Kang, Y.; Villabroza, K. R.; Liao, Y.; Chang, C. H.; Donahue, T.; Nel, A. E.; Meng, H. Irinotecan Delivery by Lipid-Coated Mesoporous Silica Nanoparticles Show Improved Efficacy and Safety over Liposomes for Pancreatic Cancer. *ACS Nano* **2016**, *10*, 2702−2715.

(8) Zhang, J.; Yuan, Z.; Wang, Y.; Chen, W.; Luo, G.; Cheng, S.; Zhuo, R.; Zhang, X. Multifunctional Envelope-Type Mesoporous Silica Nanoparticles for Tumor-Triggered Targeting Drug Delivery. *J. Am. Chem. Soc.* **2013**, *135*, 5068−5073.

(9) Meng, H.; Wang, M.; Liu, H.; Liu, X.; Situ, A.; Wu, B.; Ji, Z.; Chang, C. H.; Nel, A. E. Use of a Lipid-Coated Mesoporous Silica Nanoparticle Platform for Synergistic Gemcitabine and Paclitaxel Delivery to Human Pancreatic Cancer in Mice. *ACS Nano* **2015**, *9*, 3540−3557.

(10) Erkan, M.; Hausmann, S.; Michalski, C. W.; Fingerle, A. A.; Dobritz, M.; Kleeff, J.; Friess, H. The Role of Stroma in Pancreatic Cancer: Diagnostic and Therapeutic Implications. *Nat. Rev. Gastroenterol. Hepatol.* **2012**, *9*, 454−467.

(11) Kota, J.; Hancock, J.; Kwon, J.; Korc, M. Pancreatic Cancer: Stroma and Its Current and Emerging Targeted Therapies. *Cancer Lett.* **2017**, *391*, 38−49.

(12) Neesse, A.; Bauer, C. A.; Öhlund, D.; Lauth, M.; Buchholz, M.; Michl, P.; Tuveson, D. A.; Gress, T. M. Stromal biology and therapy in pancreatic cancer: ready for clinical translation? *Gut* **2019**, *68*, 159−171.

(13) Meng, H.; Nel, A. E. Use of nano engineered approaches to overcome the stromal barrier in pancreatic cancer. *Adv. Drug Delivery Rev.* **2018**, *130*, 50−57.

(14) Ji, T. J.; Lang, J. Y.; Wang, J.; Cai, R.; Zhang, Y. L.; Qi, F. F.; Zhang, L. J.; Zhao, X.; Wu, W. J.; Hao, J. H.; Qin, Z. H.; Zhao, Y.; Nie, G. Designing Liposomes To Suppress Extracellular Matrix Expression To Enhance Drug Penetration and Pancreatic Tumor Therapy. *ACS Nano* **2017**, *11*, 8668−8678.

(15) Stylianopoulos, T.; Jain, R. K. Combining Two Strategies to Improve Perfusion and Drug Delivery in Solid Tumors. *Proc. Natl. Acad. Sci. U. S. A.* **2013**, *110*, 18632−18637.

(16) Bhaw-Luximon, A.; Jhurry, D. New Avenues for Improving Pancreatic Ductal Adenocarcinoma (PDAC) Treatment: Selective Stroma Depletion Combined with Nano Drug Delivery. *Cancer Lett.* **2015**, *369*, 266−273.

(17) Zhao, R. F.; Han, X. X.; Li, Y. Y.; Wang, H.; Ji, T. J.; Zhao, Y. L.; Nie, G. J. Photothermal Effect Enhanced Cascade-Targeting Strategy for Improved Pancreatic Cancer Therapy by Gold Nanoshell@Mesoporous Silica Nanorod. *ACS Nano* **2017**, *11*, 8103−8113.

(18) Pei, Y. Y.; Chen, L.; Huang, Y. K.; Wang, J. H.; Feng, J. X.; Xu, M. J.; Chen, Y.; Song, Q. X.; Jiang, G.; Gu, X.; Zhang, Q.; Gao, X. L.; Chen, J. Sequential Targeting TGF-β Signaling and KRAS Mutation Increases Therapeutic Efficacy in Pancreatic Cancer. *Small* **2019**, *15*, 1900631.

(19) Chen, X. L.; Zhou, W. X.; Liang, C.; Shi, S.; Yu, X. J.; Chen, Q. J.; Sun, T.; Lu, Y. F.; Zhang, Y. J.; Guo, Q.; Li, C.; Zhang, Y.; Jiang, C. CodeliveryNanosystem Targeting the Deep Microenvironment of Pancreatic Cancer. *Nano Lett.* **2019**, *19*, 3527−3534.

(20) Meng, H.; Wang, M. Y.; Liu, H. Y.; Liu, X. S.; Situ, A.; Wu, B.; Ji, Z. X.; Chang, C. H.; Nel, A. E. Use of a Lipid-Coated Mesoporous Silica Nanoparticle Platform for Synergistic Gemcitabine and Paclitaxel Delivery to Human Pancreatic Cancer in Mice. *ACS Nano* **2015**, *9*, 3540−3557.

(21) Han, X. X.; Li, Y. Y.; Xu, Y.; Zhao, X.; Zhang, Y. L.; Yang, X.; Wang, Y. W.; Zhao, R. F.; Anderson, G. J.; Zhao, Y. L.; Nie, G. J. Reversal of Pancreatic Desmoplasia by Re-educating Stellate Cells with a Tumour Microenvironment-activated Nanosystem. *Nat. Commun.* **2018**, *9*, 3390.

(22) Xuan, W. J.; Xia, Y. H.; Li, T.; Wang, L. L.; Liu, Y. L.; Tan, W. H. Molecular Self-Assembly of BioorthogonalAptamer-Prodrug Conjugate Micelles for Hydrogen Peroxide and pH-Independent Cancer Chemodynamic Therapy. *J. Am. Chem. Soc.* **2020**, *142*, 937−944.

(23) Li, J. C.; Huang, J. G.; Lyu, Y.; Huang, J. S.; Jiang, Y. Y.; Xie, C.; Pu, K. Y. Photoactivatable Organic Semiconducting Pro-nanoenzymes. *J. Am. Chem. Soc.* **2019**, *141*, 4073−4079.

(24) Cui, D.; Huang, J. G.; Zhen, X.; Li, J. C.; Jiang, Y. Y.; Pu, K. Y. A Semiconducting Polymer Nano-prodrug for Hypoxia-Activated Photodynamic Cancer Therapy. *Angew. Chem., Int. Ed.* **2019**, *58*, 5920−5924.

(25) Li, J. C.; Xie, C.; Huang, J. G.; Jiang, Y. Y.; Miao, Q. Q.; Pu, K. Y. Semiconducting Polymer Nanoenzymes with Photothermic Activity for Enhanced Cancer Therapy. *Angew. Chem., Int. Ed.* **2018**, *57*, 3995−3998.

(26) Hu, K. L.; Miao, L.; Goodwin, T. J.; Li, J.; Liu, Q.; Huang, L. Quercetin Remodels the Tumor Microenvironment To Improve the Permeation, Retention, and Antitumor Effects of Nanoparticles. *ACS Nano* **2017**, *11*, 4916−4925.

(27) Sherman, M. H.; Yu, R. T.; Engle, D. D.; Ding, N.; Atkins, A. R.; Tiriac, H.; Collisson, E. A.; Connor, F.; Van Dyke, T.; Kozlov, S.; Martin, P.; Tseng, T. W.; Dawson, D. W.; Donahue, T. R.; Masamune, A.; Shimosegawa, T.; Apte, m. V.; Wilson, J. S.; Ng, B.; Lau, S. L.; Gunton, J. E.; Wahl, G. M.; Hunter, T.; Drebin, J. A.; O'Dwyer, P. J.; Liddle, C.; Tuveson, D. A.; Downes, M.; Evans, R. M. Vitamin D Receptor-Mediated Stromal Reprogramming Suppresses Pancreatitis and Enhances Pancreatic Cancer Therapy. *Cell* **2014**, *159*, 80−93.

(28) Liu, J. Q.; Liao, S.; Diop-Frimpong, B.; Chen, W.; Goel, S.; Naxerova, K.; Ancukiewicz, M.; Boucher, Y.; Jain, R. K.; Xu, L. TGF-β Blockade Improves the Distribution and Efficacy of Therapeutics in Breast Carcinoma by Normalizing the Tumor Stroma. *Proc. Natl. Acad. Sci. U. S. A.* **2012**, *109*, 16618−16623.

(29) Meng, H.; Zhao, Y.; Dong, J. Y.; Xue, M.; Lin, Y. S.; Ji, Z. X.; Mai, W. X.; Zhang, H. Y.; Chang, C. H.; Brinker, C. J.; Zink, J. I.; Nel, A. E. Two-Wave Nanotherapy To Target the Stroma and Optimize Gemcitabine Delivery to a Human Pancreatic Cancer Model in Mice. *ACS Nano* **2013**, *7*, 10048−10065.

(30) Wu, L. F.; Zhou, B.; Oshiro-Rapley, N.; Li, M.; Paulo, J. A.; Webster, C. M.; Mou, F.; Kacergis, M. C.; Talkowski, M. E.; Carr, C. E.; Gygi, S. P.; Zheng, B.; Soukas, A. A. *Cell* **2016**, *167*, 1705−1718.

(31) Birsoy, K.; Possemato, R.; Lorbeer, F. K.; Bayraktar, E. C.; Thiru, P.; Yucel, B.; Wang, T.; Chen, W. W.; Clish, C. B.; Sabatini, D. M. Metabolic Determinants of Cancer Cell Sensitivity to Glucose Limitation and Biguanides. *Nature* **2014**, *508*, 108−112.

(32) Sui, X. B.; Xu, Y. H.; Wang, X.; Han, W. D.; Pan, H. M.; Xiao, M. Metformin: A Novel but Controversial Drug in Cancer Prevention and Treatment. *Mol. Pharmaceutics* **2015**, *12*, 3783−3791.

(33) Sacco, F.; Calderone, A.; Castagnoli, L.; Cesareni, G. The Cell-autonomous Mechanisms Underlying the Activity of Metformin as an Anticancer Drug. *Br. J. Cancer* **2016**, *115*, 1451−1456.

https://dx.doi.org/10.1021/jacs.0c00650
J. Am. Chem. Soc. 2020, 142, 4944−4954

(34) Duca, F. A.; Côté, C. D.; Rasmussen, B. A.; Zadeh-Tahmasebi, M.; Rutter, G. A.; Filippi, B. M.; Lam, T. K. Metformin Activates a Duodenal Ampk-dependent Pathway to Lower Hepatic Glucose Production in Rats. *Nat. Med.* **2015**, *21*, 506−511.
(35) Storozhuk, Y.; Hopmans, S. N.; Sanli, T.; Barron, C.; Tsiani, E.; Cutz, J. C.; Pond, G.; Wright, J.; Singh, G.; Tsakiridis, T. Metformin Inhibits Growth and Enhances Radiation Response of Non-small Cell Lung Cancer (NSCLC) Through ATM and AMPK. *Br. J. Cancer* **2013**, *108*, 2021−2032.
(36) Shi, W. Y.; Xiao, D.; Wang, L.; Dong, L. H.; Yan, Z. X.; Shen, Z. X.; Chen, S. J.; Chen, Y.; Zhao, W. L. Therapeutic Metformin/AMPK Activation Blocked Lymphoma Cell Growth via Inhibition of mTOR Pathway and Induction of Autophagy. *Cell Death Dis.* **2012**, *3*, No. e275.
(37) Duan, W.; Chen, K.; Jiang, Z.; Chen, X.; Sun, L.; Li, J.; Lei, J.; Xu, Q.; Ma, J.; Li, X.; Han, L.; Wang, Z.; Wu, Z.; Wang, F.; Wu, E.; Ma, Z.; Ma, Q. Desmoplasia Suppression by Metformin-mediated AMPK Activation Inhibits Pancreatic Cancer Progression. *Cancer Lett.* **2017**, *385*, 225−233.
(38) da Silva Morais, A.; Abarca-Quinones, J.; Guigas, B.; Viollet, B.; Stärkel, P.; Horsmans, Y.; Leclercq, I. A. Development of Hepatic Fibrosis Occurs Normally in AMPK-deficient Mice. *Clin. Sci.* **2010**, *118*, 411−420.
(39) Deacon, J. C.; Engelman, D. M.; Barrera, F. N. Targeting Acidity in Diseased Tissues: Mechanism and Applications of the Membrane-inserting Peptide pHLIP. *Arch. Biochem. Biophys.* **2015**, *565*, 40−48.
(40) Jin, Q.; Deng, Y.; Chen, X.; Ji, J. Rational Design of Cancer Nanomedicine for Simultaneous Stealth surface and Enhanced Cellular Uptake. *ACS Nano* **2019**, *13*, 954−977.
(41) Janic, B.; Bhuiyan, M. P. I.; Ewing, J. R.; Ali, M. M. pH-Dependent Cellular Internalization of Paramagnetic Nanoparticle. *ACS Sens.* **2016**, *1*, 975−978.
(42) Jia, Q. J.; Zeng, J. F.; Qiao, R. R.; Jing, L. H.; Peng, L.; Gu, F. L.; Gao, M. Y. Gelification: An Effective Measure for Achieving Differently Sized Biocompatible Fe_3O_4 Nanocrystals through a Single Preparation Recipe. *J. Am. Chem. Soc.* **2011**, *133*, 19512−19523.
(43) Lim, J. Y.; Oh, M. A.; Kim, W. H.; Sohn, H. Y.; Park, S. I. AMP-activated Protein Kinase Inhibits TGF-β-induced FibrogenicResponses of Hepatic Stellate Cells by Targeting Transcriptional Coactivator p300. *J. Cell. Physiol.* **2012**, *227*, 1081−1089.
(44) Leask, A.; Abraham, D. J. TGF-β Signaling and the Fibrotic Response. *FASEB J.* **2004**, *18*, 816−827.
(45) Zhan, H. X.; Zhou, B.; Cheng, Y. G.; Xu, J. W.; Wang, L.; Zhang, G. Y.; Hu, S. Y. Crosstalk between Stromal Cells and Cancer Cells in Pancreatic Cancer: New Insights into Stromal Biology. *Cancer Lett.* **2017**, *392*, 83−93.
(46) Neesse, A.; Algül, H.; Tuveson, D. A.; Gress, T. M. Stromal Biology and Therapy in Pancreatic Cancer: a Changing Paradigm. *Gut* **2015**, *64*, 1476−1484.
(47) Hu, Q.; Sun, W.; Wang, C.; Gu, Z. Recent Advances of Cocktail Chemotherapy by Combination Drug Delivery Systems. *Adv. Drug Delivery Rev.* **2016**, *98*, 19−34.
(48) Shim, G.; Kim, M. G.; Kim, D.; Park, J. Y.; Oh, Y. K. Nanoformulation-based Sequential Combination Cancer Therapy. *Adv. Drug Delivery Rev.* **2017**, *115*, 57−81.
(49) Miao, L.; Guo, S. T.; Lin, M.; Liu, Q.; Huang, L. Nanoformulations for Combination or Cascade Anticancer Therapy. *Adv. Drug Delivery Rev.* **2017**, *115*, 3−22.
(50) Gao, ZA. Y.; Hou, Y.; Zeng, J. F.; Chen, L.; Liu, C. Y.; Yang, W. S.; Gao, M. Y. Tumor Microenvironment-Triggered Aggregation of Antiphagocytosis 99mTc-Labeled Fe_3O_4Nanoprobes for Enhanced Tumor Imaging in vivo. *Adv. Mater.* **2017**, *29*, 1701095.
(51) Ma, T. C.; Hou, Y.; Zeng, J. F.; Liu, C. Y.; Zhang, P. S.; Jing, L. H.; Shangguan, D. H.; Gao, M. Y. Dual-Ratiometric Target-Triggered Fluorescent Probe for Simultaneous Quantitative Visualization of Tumor Microenvironment Protease Activity and pH in Vivo. *J. Am. Chem. Soc.* **2018**, *140*, 211−218.
(52) Lee, G. Y.; Qian, W. P.; Wang, L. Y.; Wang, Y. A.; Staley, C. A.; Satpathy, M.; Nie, S. M.; Mao, H.; Yang, L. Theranostic Nanoparticles with Controlled Release of Gemcitabine for Targeted Therapy and MRI of Pancreatic Cancer. *ACS Nano* **2013**, *7*, 2078−2089.
(53) Valsecchi, M. E.; Díaz-Cantón, E.; de la Vega, M.; Littman, S. J. Recent Treatment Advances and Novel Therapies in Pancreas Cancer: A Review. *J. Gastrointest. Cancer* **2013**, *45*, 190−201.
(54) Provenzano, P. P.; Cuevas, C.; Chang, A. E.; Goel, V. K.; Von Hoff, D. D.; Hingorani, S. R. Enzymatic Targeting of the Stroma Ablates Physical Barriers to Treatment of Pancreatic Ductal Adenocarcinoma. *Cancer Cell* **2012**, *21*, 418−429.
(55) *A Study of PEGylated Recombinant Human Hyaluronidase in Combination With Nab-Paclitaxel Plus Gemcitabine Compared With Placebo Plus Nab-Paclitaxel and Gemcitabine in Participants With Hyaluronan-High Stage IV Previously Untreated Pancreatic Ductal Adenocarcinoma*, https://clinicaltrials.gov/ct2/show/NCT02715804?term=halozyme+301&rank=1.
(56) Frese, K. K.; Neesse, A.; Cook, N.; Bapiro, T. E.; Lolkema, M. P.; Jodrell, D. I.; Tuveson, D. A. nab-Paclitaxel Potentiates Gemcitabine Activity by Reducing Cytidine Deaminase Levels in a Mouse Model of Pancreatic Cancer. *Cancer Discovery* **2012**, *2*, 260−269.
(57) Von Hoff, D. D.; Ervin, T.; Arena, F. P.; Chiorean, E. G.; Infante, J.; Moore, M.; Seay, T.; Tjulandin, S. A.; Ma, W. W.; Saleh, M. N.; Harris, M.; Reni, M.; Dowden, S.; Laheru, D.; Bahary, N.; Ramanathan, R. K.; Tabernero, J.; Hidalgo, M.; Goldstein, D.; Van Cutsem, E.; Wei, X.; Iglesias, J.; Renschler, M. K. Increased Survival Inpancreatic Cancer with nab-paclitaxel plus Gemcitabine. *N. Engl. J. Med.* **2013**, *369*, 1691−1703.
(58) Lee, J.; Yesilkanal, A. E.; Wynne, J. P.; Frankenberger, C.; Liu, J.; Yan, J.; Elbaz, M.; Rabe, D. C.; Rustandy, F. D.; Tiwari, P.; Grossman, E. A.; Hart, P. C.; Kang, C.; Sanderson, S. M.; Andrade, J.; Nomura, D. K.; Bonini, M. G.; Locasale, J. W.; Rosner, M. R. Effective Breast Cancer Combination Therapy Targeting BACH1 and Mitochondrial Metabolism. *Nature* **2019**, *568*, 254−258.
(59) DeWaal, D.; Nogueira, V.; Terry, A. R.; Patra, K. C.; Jeon, S. M.; Guzman, G.; Au, J.; Long, C. P.; Antoniewicz, M. R.; Hay, N. Hexokinase-2 Depletion Inhibits Glycolysis and Induces Oxidative Phosphorylation in Hepatocellular Carcinoma and Sensitizes to Metformin. *Nat. Commun.* **2018**, *9*, 446.
(60) Rangarajan, S.; Bone, N. B.; Zmijewska, A. A.; Jiang, S.; Park, D. W.; Bernard, K.; Locy, M. L.; Ravi, S.; Deshane, J.; Mannon, R. B.; Abraham, E.; Darley-Usmar, V.; Thannickal, V. J.; Zmijewski, J. W. Metformin Reverses Established Lung Fibrosis in a Bleomycin Model. *Nat. Med.* **2018**, *24*, 1121−1127.
(61) Kheirollahi, V.; Wasnick, R. M.; Biasin, V.; Vazquez-Armendariz, A. I.; Chu, X.; Moiseenko, A.; Weiss, A.; Wilhelm, J.; Zhang, J. S.; Kwapiszewska, G.; Herold, S.; Schermuly, R. T.; Mari, B.; Li, X.; Seeger, W.; Günther, A.; Bellusci, S.; El Agha, E. Metformin Induces Lipogenic Differentiation in Myofibroblasts to Reverse Lung Fibrosis. *Nat. Commun.* **2019**, *10*, 2987.
(62) Shankaraiah, R. C.; Callegari, E.; Guerriero, P.; Rimessi, A.; Pinton, P.; Gramantieri, L.; Silini, E. M.; Sabbioni, S.; Negrini, M. Metformin Prevents Liver Tumourigenesis by Attenuating Fibrosis in a Transgenic Mouse Model of Hepatocellular Carcinoma. *Oncogene* **2019**, *38*, 7035−7045.

https://dx.doi.org/10.1021/jacs.0c00650
J. Am. Chem. Soc. 2020, 142, 4944−4954